Morphing Compression Garments for Space Medicine and Extravehicular Activity Using Active Materials

Bradley T. Holschuh; Dava J. Newman

INTRODUCTION: Compression garments tend to be difficult to don/doff, due to their intentional function of squeezing the wearer. This is especially true for compression garments used for space medicine and for extravehicular activity (EVA). We present an innovative solution to this problem by integrating shape changing materials—NiTi shape memory alloy (SMA) coil actuators formed into modular, 3D-printed cartridges—into compression garments to produce garments capable of constricting on command.

METHODS: A parameterized, 2-spring analytic counterpressure model based on 12 garment and material inputs was developed to inform garment design. A methodology was developed for producing novel SMA cartridge systems to enable active compression garment construction. Five active compression sleeve prototypes were manufactured and tested: each sleeve was placed on a rigid cylindrical object and counterpressure was measured as a function of spatial location and time before, during, and after the application of a step voltage input.

RESULTS: Controllable active counterpressures were measured up to 34.3 kPa, exceeding the requirement for EVA life support (29.6 kPa). Prototypes which incorporated fabrics with linear properties closely matched analytic model predictions (4.1%/−10.5% error in passive/active pressure predictions); prototypes using nonlinear fabrics did not match model predictions (errors >100%). Pressure non-uniformities were observed due to friction and the rigid SMA cartridge structure.

DISCUSSION: To our knowledge this is the first demonstration of controllable compression technology incorporating active materials, a novel contribution to the field of compression garment design. This technology could lead to easy-to-don compression garments with widespread space and terrestrial applications.

KEYWORDS: extravehicular activity, mechanical counterpressure space suit, orthostatic intolerance, wearable technology, shape memory alloys.

Holschuh BT, Newman DJ. *Morphing compression garments for space medicine and extravehicular activity using active materials*. Aerosp Med Hum Perform. 2016; 87(2):84–92.

Compression garments serve many useful purposes for millions of people in their everyday lives. Beyond their traditional use as treatments for lymphedema,[7] venous insufficiency,[10] burn injuries,[29] and other medical/cosmetic/athletic applications,[11] compression therapies can serve as critical life support devices in battlefield scenarios,[21] as well as protect astronauts in space against the vacuum environment[24] and prevent orthostatic intolerance once they return to Earth.[25,27,28] A specific example of high-performance extreme environment compression garments—mechanical counterpressure (MCP) space suits such as the Space Activity Suit (1971) and the MIT BioSuit™ (2005-present)—are high-mobility space suits designed to protect astronauts during extravehicular activity (EVA) by imparting 29.6 kPa counterpressure across the entire body in the vacuum of space (upwards of 10× the typical compression required of a medical grade compression stocking).[19,31,32]

Compression garments typically take one of two forms: a passive garment, undersized relative to the wearer, that produces compression due to stretching of the garment once donned (e.g.,

From the Department of Aeronautics and Astronautics, Massachusetts Institute of Technology, Cambridge, MA.

This manuscript was received for review in April 2015. It was accepted for publication in October 2015.

Address correspondence to: Bradley T. Holschuh, Ph.D., Department of Aeronautics and Astronautics, MIT, 77 Massachusetts Ave., Rm. 37-331, Cambridge, MA 02139; holschuh@mit.edu.

DOI: 10.3357/AMHP.4349.2016

a typical, commercially available, medical-grade stocking, or the Russian Kentavr, worn by cosmonauts to prevent orthostatic intolerance);[25] or an inflatable sleeve that fills with pressurized gas to squeeze the wearer once donned [e.g., intermittent pneumatic compression sleeves used to improve circulation, or the NASA inflatable antigravity suit (AGS), also used to prevent orthostatic intolerance].[7,25] Because they are designed to intentionally squeeze the wearer, compression garments can be either bulky/cumbersome (if using bladders/pumps) or difficult to don/doff (if the user is required to stretch an undersized stocking over their limbs), limiting their ultimate usability. For these reasons, compression garment design will greatly benefit from modern wearable technology, specifically shape-changing materials (sometimes referred to as artificial muscles),[23] which if strategically integrated into a garment may enable active manipulation of the garment materials with low mass and low bulk. Previous research has identified shape memory alloy (SMA) coil actuators as ideal materials for use in actively controlled compression garments like MCP space suits for planetary exploration of the Moon or Mars.[16,17,24] In this paper, we expand on previous research on this topic and present the design and development of a novel active compression system using SMA actuators integrated into a simplistic cuff-like garment. We first present an expanded analytic model for compression garments incorporating SMA actuators; then we present the development of modular, 3D-printed SMA actuator cartridges necessary for design implementation; and finally, we demonstrate the ability of the garment to produce dynamic, controllable counterpressure at levels sufficient for MCP exploration activities, suggesting a new design frontier for compression garments.

SMA spring actuators contract when heated due to solid state martensite-to-austenite phase transformations[2,20,22] and have been shown to produce large forces and displacements with spring diameters as small as 1.24 mm.[14,17,26] SMAs have been previously integrated into wearable garments[1,6,33] and have even been demonstrated in compression garment settings.[17] NiTi is the most commonly used SMA material, though a variety of alloys exist that exhibit this functionality.[22]

The most basic architecture to produce a compression garment using SMA coil actuators is a hybrid configuration: a passive fabric strip, connected at the seam to SMA actuators, forming a circular cuff structure that can be wrapped circumferentially around an object (see **Fig. 1**).[15,17] As the actuators trigger, the cuff constricts, stretching the passive fabric and producing tension that imparts a pressure to the underlying object.

We previously suggested this architecture concept and derived an analytic model to predict passive and active counterpressures based on 12 design variables.[15,17] Specifically, active and passive pressures (P_P and P_A) are calculated using the following equations (see **Table I** for definitions and typical values of each parameter):

$$P_P = \left(\frac{Et}{r}\right)\left(\frac{2\pi r - L_{S0}\left(1+\varepsilon_{S\max}\right)}{L_{F0}} - 1\right); \qquad \text{Eq. 1}$$

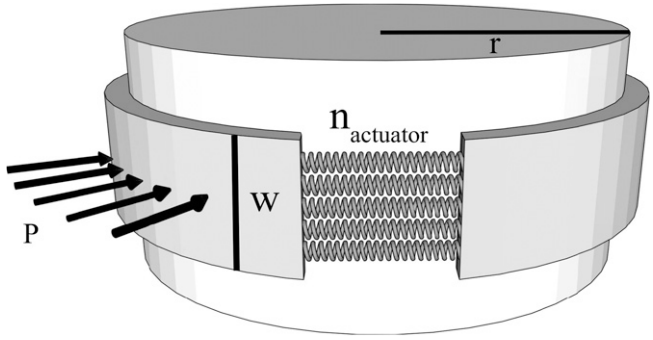

Fig. 1. Illustration of hybrid SMA compression sleeve concept, combining a passive fabric strip with several SMA spring actuators. This architecture was previously proposed in Holschuh and Newman[15] and Holschuh et al.[17]

$$P_A = \frac{\Delta X_{System} G_A d^2 n_a Et}{r\left(G_A d^2 n_a L_{F0} + 8EwtC^3\eta L_{S0}\right)}. \qquad \text{Eq. 2}$$

Using these equations, it is possible to design compression garments to achieve any number of performance requirements by tailoring specific garment characteristics (e.g., maximizing active counterpressure with minimum passive counterpressure for a given passive elastic material, maximizing percentage fabric coverage or minimizing garment thickness for a minimum pressure active pressure target, etc.). Select design studies have been previously detailed.[15]

We further develop these equations to identify designs specifically tailored for MCP space suit applications. The three prevailing design requirements for MCP suits—0 kPa passive pressure (for easy donning/doffing), 29.6 kPa active pressure (for EVA life

Table I. Analytical Pressure Production Model Inputs and Outputs, with Typical Values Presented for a 1-cm Wide Active Sleeve Sized for a Human Thigh.

PARAMETER	UNITS	TYPICAL VALUE	DESCRIPTION
C	–	3	SMA spring index (D/d)
d	m	$305 * 10^{-6}$	SMA wire diameter
E	Pa	$1.4 * 10^{6}$	Passive fabric Young's Modulus
ϵ_{Smax}	–	3	Maximum SMA de-twinned extensional strain
G_A	Pa	$25 * 10^{9}$	SMA austenite shear modulus
η	–	0.9	SMA spring packing density
L_{F0}	m	$27 * 10^{-2}$	Passive fabric unstretched length
L_{S0}	m	$8 * 10^{-2}$	SMA twinned-martensite length
n_a	–	8	Number of parallel actuators in system
r	m	$9.5 * 10^{-2}$	Limb radius
t	m	$4.9 * 10^{-3}$	Passive fabric material thickness
w	m	$1 * 10^{-2}$	Passive fabric axial width
ΔX_{System}	m	$24.7 * 10^{-2}$	Unstretched system closure gap ($2\pi r - (L_{S0} + L_{F0})$)
P_P	Pa	$1.85 * 10^{3}$	Passive counterpressure
P_A	Pa	$54.5 * 10^{3}$	Active counterpressure

Holschuh and Newman (2015).[15]

support), and thickness less than 5 mm (for wearability)—can be used to set constraints on Eqs. 1 and 2. For a hypothetical thigh compression sleeve designed with the garment parameters presented in Table I, we can simultaneously vary the SMA twinned length (L_{S0}), the unstretched fabric length (L_{F0}), and the material thickness (t), to generate contours of constant passive and active pressure that meet these requirements using Eqs. 1 and 2. This is shown in **Fig. 2**: the lighter surface represents the complete design space that produces a garment with 0 kPa passive pressure; the darker surface represents the complete design space that produces a garment with 30-kPa active pressures. The intersection of the contours in Fig. 2 (identified by the black curve) is a 3-dimensional curve which represents the complete matrix of design solutions D (i.e., every L_{S0}, L_{F0}, and t triad) that satisfies all MCP design requirements. Mathematically, we express this 3-dimensional curve by parameterizing Eqs. 1 and 2 for each dimension (L_{S0}, L_{F0}, and t) using a chosen parameter (τ):

$$L_{S0}(\tau_i) = \tau_i; \quad \text{Eq. 3}$$

$$L_{F0}(\tau_i) = 2\pi r - \tau_i(1+\varepsilon_{S\max}); \quad \text{Eq. 4}$$

$$t(\tau_i) = \frac{P_A r d^2 G_A n_a (2\pi r - \tau_i(1+\varepsilon_{S\max}))}{\tau_i E(G_A d^2 n_a \varepsilon_{S\max} - 8P_A r w C^3 \eta)}; \quad \text{Eq. 5}$$

$$\mathbf{D} = \begin{array}{c} \\ \tau_1 \\ \tau_2 \\ \vdots \\ \tau_n \end{array} \begin{array}{c} \begin{array}{ccc} L_{S0} & L_{F0} & t \end{array} \\ \begin{pmatrix} L_{S0}(\tau_1) & L_{F0}(\tau_1) & t(\tau_1) \\ L_{S0}(\tau_2) & L_{F0}(\tau_2) & t(\tau_2) \\ \vdots & \vdots & \vdots \\ L_{S0}(\tau_n) & L_{F0}(\tau_n) & t(\tau_n) \end{pmatrix} \end{array}$$

where

$$0 < \tau_1 \ldots \tau_n < \frac{2\pi r}{1+\varepsilon_{S\max}}; \quad \text{Eq. 6}$$

$$t(\tau_n) \leq 5 \text{ mm}. \quad \text{Eq. 7}$$

METHODS

Prototype Construction

A critical first step in developing active compression garments using SMA actuators is to design a packaging solution for the SMA actuators themselves. While individual actuators have been shown to produce sizable forces when exposed to an applied voltage,[17] the magnitude of force required for MCP applications can only be achieved when several actuators are aligned in parallel. In such a configuration, it is advantageous to minimize the wasted space between actuators (i.e., to pack them as close together as possible) because this maximizes the total force produced per unit width (producing the greatest counterpressure). However, this introduces new design challenges: preventing the actuators from short-circuiting; sufficiently fixing the actuators in place to prevent structural failure (e.g., an actuator breaking free) during activation (especially at high tension/pressure levels); and successfully pairing the actuators to the passive fabric.

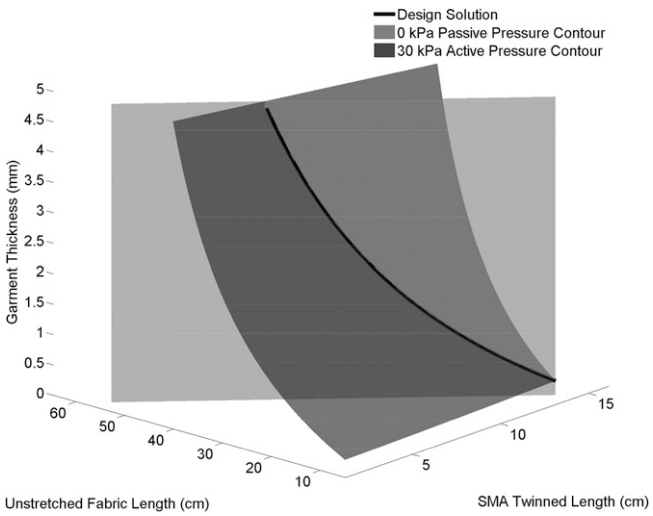

Fig. 2. Two-spring model output for theoretical thigh sleeve. Surfaces representing contours of constant pressure are shown for the 0-kPa passive pressure condition and the 30-kPa active pressure condition. The line formed by the intersection of these surfaces represents the design space that satisfies both EVA life support requirements and simple donning/doffing requirements.

A cartridge-style SMA structure incorporating a singular, extended, and de-twinned SMA spring into 3D-printed end caps and a central spacer was developed to address this issue (see **Fig. 3**, top left panel, for an example of this design). In this configuration, one SMA spring is laced between two end caps and one central spacing element 12 times, resulting in an actuator with 12 effective parallel springs that are equally spaced. Because the cartridge is comprised of a singular actuator (instead of 12 individual actuators), both electrical conductivity and actuator structural integrity are guaranteed (i.e., the series circuit cannot be compromised unless the actuator wire breaks and no actuators can individually pull free of the structure, barring failure of the wire or end cap structure itself). Further, given the flexibility in design of the 3D-printed end caps, a variety of designs are possible for pairing the cartridge to the adjoining passive fabrics.

Two methods for manufacturing these cartridge actuators were developed based on current additive manufacturing capability: a single-plastic method, where the SMA actuator is fully encased in homogeneous ABS plastic end caps in a single step, achieved by pausing the 3D printing build phase part-way through the process to embed the actuator (created using a Stratasys Fortus 250mc printer; Stratasys, Ltd., Eden Prairie, MN); and a multiplastic method, where end-cap insets are prefabricated using a high temperature plastic (such as Stratasys ULTEM*

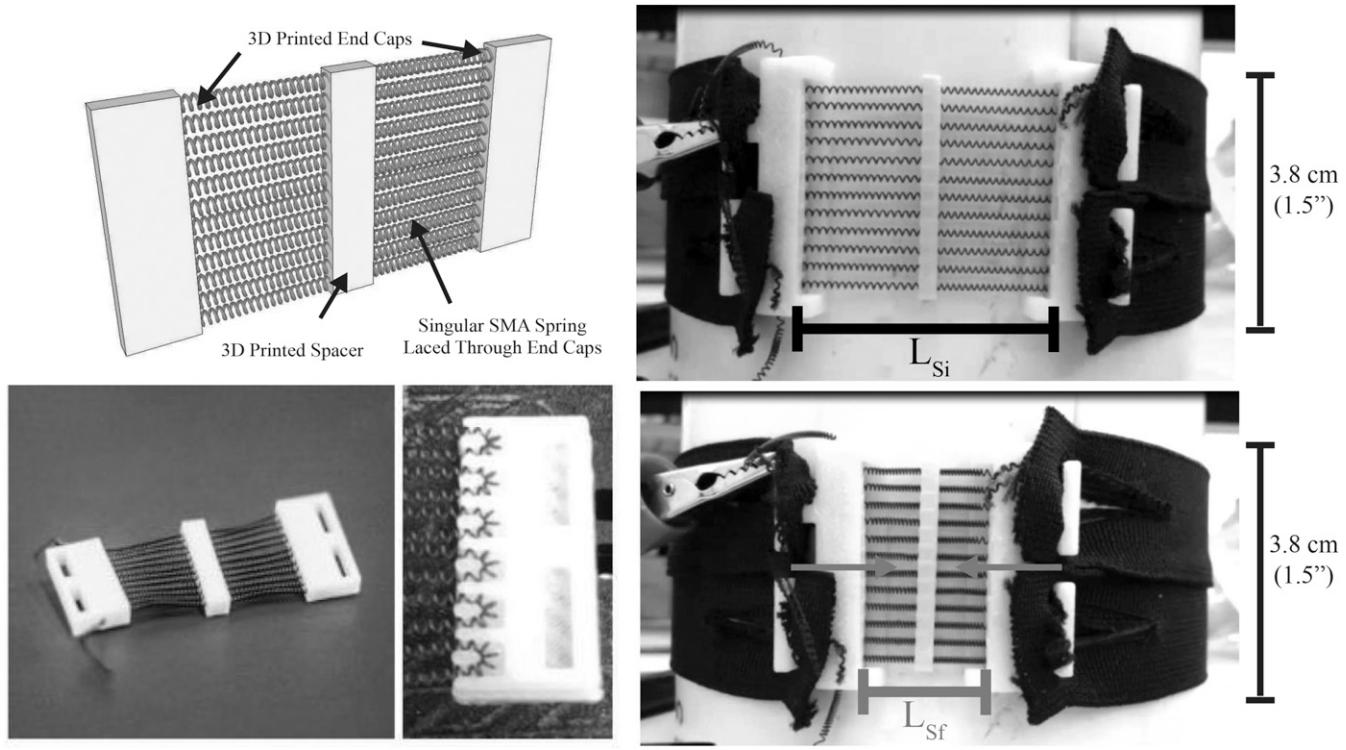

Fig. 3. Modular, 3D-printed SMA cartridge concept, prototype, and activation stroke. Top left: SMA cartridge concept with 3D printed end caps and central spacer. Bottom left: 2.5 cm (1") wide single-plastic SMA cartridge prototype, with cut away of end cap structure shown. Cartridge is comprised of a single SMA actuator laced between end caps midway through the 3D printing process, creating a modular cartridge structure with several parallel actuators. Top and bottom right: 3.8 cm (1.5") multiplastic SMA cartridge paired with passive fabric in a cuff-like sleeve configuration, shown pre- and post-activation (compression stroke illustrated in dark grey). Prototypes produced and tested in this study were of comparable size and configuration to this cuff.

9085) and the SMA spring is loosely laced through these pieces then finished in ABS end-cap superstructures (created using both Stratasys Fortus 400mc and Stratasys Fortus 250mc printers). An example of a cartridge produced using the single-plastic method (including the lacing-step midway through the print process), is included in Fig. 3, bottom left panel, and an example of this cartridge, paired with a passive fabric to form a 3.8-cm wide (1.5") cuff-like sleeve, is shown pre- and post-activation in Fig. 3, right two panels. All SMA cartridges used in this study were produced using the multiplastic method, which was found to have greater thermal stability than the single-plastic method.

Procedure

Nine counterpressure tests were conducted using five different cuff-like sleeve prototypes that were produced in house (spanning a variety of design parameters, enumerated in detail in **Table II**). Each sleeve was comprised of a passive fabric section paired with a SMA multiplastic actuator cartridge containing 12 SMA actuator segments. Sleeves were made from one of two materials (jumbo spandex or generic spandex), with a variety of lengths and layers (enumerated in **Table III**). Two SMA cartridges, one for the set of jumbo spandex tests and a second for the set of generic spandex tests, were manufactured and tested.

The following protocol was implemented for each test: a sleeve was donned on a PVC cylinder ($r = 5.7$ cm) and passive and active pressures were measured as a function of time and spatial location before, during, and after the application of a voltage step input (tests were conducted at room temperature). Consistent power settings (20.3 V, 0.6 A, 12.2 W, corresponding to the maximum power setting that could be accommodated by the SMA cartridge before structural failure) were used for each test, and power was applied for approximately 60 s to allow the system to achieve steady state. Passive and active pressure data were collected using a Novel Pliance pressure system (Novel Electronics, Inc., Munich, Germany) with a custom S2075 Pliance pressure sensor mat (15.24 cm × 15.24 cm sensor with 256 sensing pixels organized into 16 rows and 16 columns, a

Table II. Summary of Design Parameters for Prototype Jumbo and Generic Spandex Tourniquet Prototypes Used in Tests 1-8.

PARAMETER	TESTS 1-4	TESTS 5-8
Spring Index C	3	3
SMA Wire Diameter d	305 μm	305 μm
Fabric Type	Jumbo Spandex	Generic Spandex
Fabric Modulus E	0.81 MPa	0.20 MPa
Maximum SMA Extensional Strain ϵ_{Smax}	3	3
SMA Shear Modulus G_A	7.5 GPa	7.5 GPa
Packing Density η	0.9	0.9
Unstretched Fabric Length L_{F0}	20.3-22.9 cm	21.4-22.9 cm
SMA Twinned Length L_{S0}	2.1 cm	1.9 cm
Number of Actuators n_a	12	12
Local Radius r	5.7 cm	5.7 cm
Fabric Layers	5-7	5-7
Total Sleeve Thickness *t*	3.5-4.9 mm	3.5-4.9 mm
Fabric Width w	3.8 cm	3.8 cm

Table III. Summary of Test Parameters for Nine Active Tourniquet Characterization Tests.

TEST	PROTOTYPE NUMBER	MATERIAL	L_{F0} (cm)	LAYERS	SENSOR LOCATION	MODIFICATIONS
1	1	Jumbo Spandex	20.3	5	Far-field	None
2	1	Jumbo Spandex	21.6	5	Far-field	Reduced friction
3	2	Jumbo Spandex	22.3	5	Far-field	Reduced friction
4	3	Jumbo Spandex	22.9	3	Far-field	Reduced friction
5	4	Generic Spandex	21.4	5	Far-field	None
6	4	Generic Spandex	21.4	5	Near-field	None
7	4	Generic Spandex	21.4	5	Far-field	Reduced friction
8	5	Generic Spandex	22.9	7	Far-field	Reduced friction
9	1	Jumbo Spandex	21.6	5	Far-field	Maximum power

range of 2-200 kPa and accuracy >95% of the measured value). Tests were conducted with the pressure sensor placed in one of two possible regions: centered exactly opposite the SMA actuator cartridge (defined as the "far-field" region); or centered exactly underneath the SMA actuator cartridge (defined as the "near-field" region). The full set of experimental parameters (prototype number, sensor location, and any test modifications) selected for each test are also included in Table III. No human subjects were tested in this experiment.

Two test pairings (1/2 and 5/7) were repeated tests with the same prototype, with low friction modifications (i.e., petroleum jelly liberally applied between the sleeve and the PVC pipe) implemented on the repeated test. This was done to determine the effect of friction on the spatial pressure profile. Subsequent tests incorporated the low-friction modification from the outset, once friction effects were determined to be problematic (see the Results and Discussion for more information on this effect). Test 9, which reused the prototype from tests 1-2, was conducted to push the system to mechanical failure to assess both the maximum pressure possible given current manufacturing techniques and to identify failure modes of the system for future improvement. For this test, the same power settings (20.3 V, 0.6 A, 12.2 W) used in previous tests were first applied to the system at t = 15 s; this power was increased at t = 90 s to 27 W (30.0 V, 0.9 A).

RESULTS

The results from these tests are summarized in **Table IV**. "Far-field" active pressures were measured up to 34.3 kPa, with increases ranging from 55.5 to 151.1% over their starting passive pressures. Settling times (defined as the time required for the powered system to achieve 90% of the steady state active pressure value) ranged from 9 s to 49 s. The analytical model accurately described the performance of the jumbo spandex sleeve (with average passive pressure errors = 4.1% and average active pressure errors = −10.5%), but failed to accurately describe the performance of the generic spandex sleeve (with average passive pressure errors = −135.5% and average active pressure errors = −168.4%).

The data from two specific tests shown in **Fig. 4**—test 3 (a low-friction jumbo spandex test) and test 9 (the maximum pressure test)—exemplify the performance seen in all other tests. In the left plot (test 3), the average sleeve pressure (i.e., the average of all sensor elements at a given time step) is presented as a function of time, with 95% confidence intervals included, for the complete "far-field" region. Power onset and removal triggers are identified, and passive and active pressure estimates are also presented, and were calculated based on experimentally determined fabric and SMA values. In the right plot (test 9), the same data is presented with each power step input identified. We identify the pressure thresholds necessary for a MCP exploration space suit (29.6 kPa) and the maximum pressure magnitude achieved (34.3 kPa). The cartridge ultimately failed at t = 139 s.

In general, the system dynamics are consistent with expectations and with the known voltage-force displacement behavior of SMA actuators (e.g., immediate rise in pressure after the voltage step input, equalizing to a steady state value, followed by a slow decay once power is removed). We see in the jumbo spandex test that the analytic pressure production model accurately predicts both passive pressure (error = −0.5%) and active pressure (error = −13.6%). The steady state pressure value depends on and, therefore, can be controlled by, the magnitude of power applied to the system. This is consistent with expectations, as the SMA force-response maps directly to a wide temperature band,[17] and the system temperature maps directly to a wide power input band.

This power dependency is captured analytically through

Table IV. Active Sleeve Test Results: Average Passive and Active "Far-Field" Pressures and Model Errors.

TEST	MEASURED P_P (kPa)	MODEL ERROR	MEASURED P_A (kPa)	MODEL ERROR
1	18.6 ± 1.1	1.1%	29.0 ± 5.7	−17.1%
2	14.3 ± 1.3	1.3%	24.8 ± 3.0	−18.0%
3	12.6 ± 0.9	-0.5%	21.9 ± 2.5	−13.6%
4	13.0 ± 0.6	14.5%	21.5 ± 1.7	6.8%
	Average Error	4.1%	Average Error	−10.5%
5	16.7 ± 1.8	−305.1%	27.1 ± 5.8	−324.8%
6	10.9 ± 5.5	N/A	18.0 ± 10.8	N/A
7	8.3 ± 0.8	−102.6%	14.9 ± 2.7	−133.4%
8	4.2 ± 0.7	1.1%	10.5 ± 1.0	−47.1%
	Average Error	−135.5%	Average Error	−168.4%
9	16.3 ± 1.3		34.3 ± 4.2	

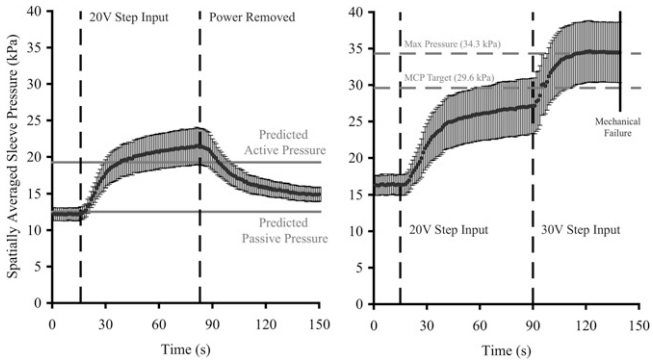

Fig. 4. Average "far-field" pressure vs. time for two representative sleeve tests. Left: 5-layer, low friction jumbo spandex sleeve average pressure vs. time over an approximate thigh radius for a 20.3-V voltage step input, with 95% confidence intervals. Predicted active and passive pressures are included based on estimated fabric modulus. Right: jumbo spandex sleeve average far-field pressure vs. time over the same radius for multiple voltage step inputs (20.3 V, 30.0 V), with 95% confidence intervals.

the SMA shear modulus term, which varies depending on the relative martensite-austenite ratio in the material. Of additional interest is the spatial variability of the pressure profile before and after activation. This data is presented in **Fig. 5** and represents data collected over two different tests (to provide a full 360° picture of the pressure distribution). In this figure, average pressure vs. spatial location for both active and passive steady state pressures are presented (with each radial position corresponding to the average pressure at that sensor element location). A top-down view of the sleeve orientation, including the relative placement of the SMA cartridge, is also provided.

In the "near-field" region, we clearly see pressure distortions caused by the SMA cartridge structures in the lower hemisphere, producing three large pressure spikes (corresponding to the two end caps and the center spacing structure), as well as under-pressures generated in the gaps between these structures (where the SMA actuators only slightly contact the surface). Interestingly, we see that the left SMA end cap shifts one location counterclockwise during activation, indicative of the SMA cartridge contraction stroke. The "far-field" pressure is more continuous, though still variable (with lower pressures measured exactly opposite the SMA cartridge). The variability in the "far-field" data is indicative of unequal stretching of the sleeve system due to high friction.

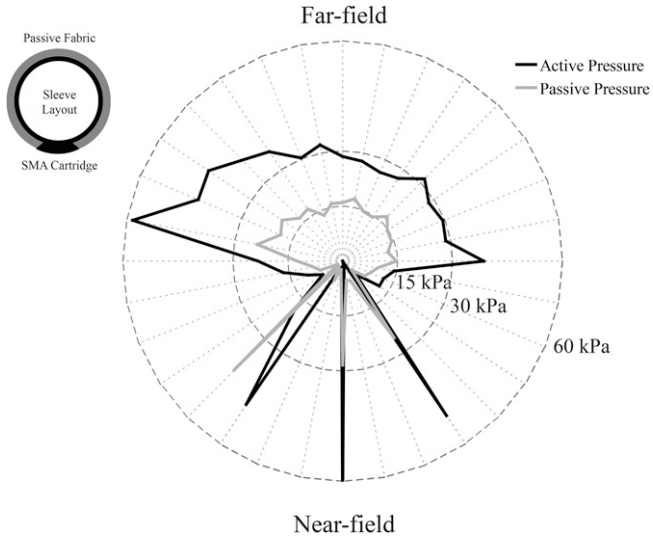

Fig. 5. Example of spatial variability of passive and active pressures (visualized as a top-down view, with the SMA cartridge located in the lower hemisphere). "Near-field" refers to the region under and near the SMA cartridge; "Far-field" refers to the region opposite the SMA cartridge. Pressure vs. spatial location is shown (with each radial position corresponding to the average pressure at that sensor element location). Contours of constant pressure, including the approximate target pressure (30 kPa), are identified.

DISCUSSION

The analytic pressure model assumes linear fabric stress-strain behavior; however, it was noted during initial fabric characterization tests and selection that only the jumbo spandex behaved linearly (up to 200% stretch), while the generic spandex behaved nonlinearly at as low as 40% stretch.[18] As shown in Table IV, the model produced accurate results when describing linear fabric systems with a stable modulus (e.g., jumbo spandex), and produced large errors when nonlinear fabrics were used (e.g., generic spandex). This issue is particularly clear when examining the results from Test 5 (generic spandex with no friction modifications): the extremely nonlinear behavior of the fabric, coupled with the high friction between the sleeve and the sensor/pipe, created local areas of extreme stretching (and therefore extremely nonlinear stress-strain responses), creating much higher pressures than the model predicted (resulting in errors >300%).

The SMA cartridge design introduces significant and unavoidable variabilities in the "near-field" spatial pressure distribution. Namely, it creates over-pressures at the locations of its structures and under-pressures both at the actuator locations and at the fabric locations immediately adjacent to the cartridge end caps. These discontinuities do not exist in the "far-field," where we observe highly continuous pressure distributions. This implication is significant from a design perspective; it is critical that the footprint of the SMA cartridge be minimized to minimize this "near-field" effect. Modifications to the SMA cartridge design or the introduction of a padded undergarment to better distribute the point loads may prove helpful in minimizing this effect.

To quantitatively judge the variability in the passive and active spatial pressure distributions in the "far-field," normalized residuals were calculated at each sensor element location for all tests (the Novel sensor contained 16 sensor element columns across its span, which we number 1-16 according to the convention presented in **Fig. 6**). These residuals (calculated as the difference between the steady-state pressure measurement at a given sensor element and the average "far-field" sleeve pressure for that test normalized by the average pressure) enable us to visualize global spatial variance trends and to determine whether nonzero correlations exist between sensor element number and passive and/or active counterpressure. The results

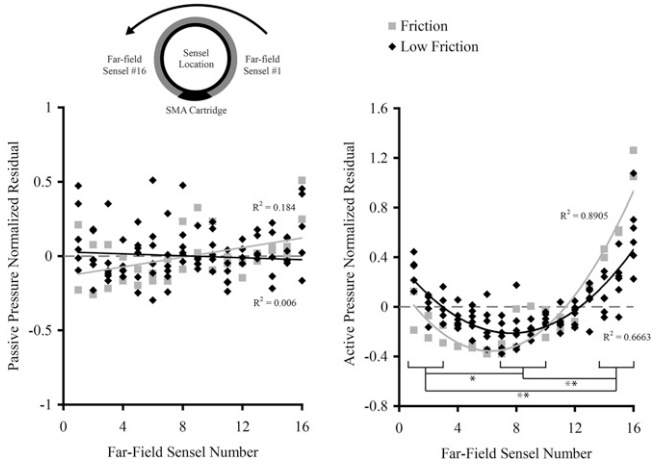

Fig. 6. Aggregate normalized passive (left) and active (right) pressure residuals vs. sensor element (sensel) number for all "far-field" pressure tests grouped into low-friction and high-friction categories. Best-fit estimates and R^2 values for each group are included, with significant ($P < 0.05$) differences identified.

of this analysis are aggregated for all "far-field" tests and are presented in both panels of Fig. 6. Best-fit estimates for each data set (passive and active pressure, low- and high-friction test setup) are also provided.

No statistically significant effects ($P < 0.05$) are observed between sensor element groups (1-3, 7-10, and 13-16) in the passive pressure data: the normalized residuals are uncorrelated with spatial location for both the low- and high-friction tests. However, significant effects ($P < 0.05$) are observed in the active pressure data when comparing the same sensor element groups: pressure is statistically lowest at the center of the field (sensor elements 7-10) and highest at the edges (sensor elements 1-3 and 14-16), and this is true in both the low- and high-friction tests.

We see some evidence that friction modifications affect the spatial pressure profile as judged by the aggregate normalized residual values in the active pressure condition (i.e., the best-fit line of the low-friction dataset is less skewed than the best-fit line of the high-friction dataset); however, the statistically significant effects previously observed were still present in both high- and low-friction conditions for all but one pairing (between sensor element groups 1-3 and 7-10 in the low-friction tests). These findings may suggest that the addition of a lubricant contributes to a more uniform pressure distribution during activation, but is insufficient on its own to mitigate the full nonuniformity in sleeve tension as the fabric stretches.

Mitigating the observed spatial pressure variability likely requires a reduction in friction between the sleeve and the underlying object. This is a problem that is intrinsic to pressure garments: friction is a function of both normal force and the local coefficient of friction, and pressure garments by definition seek to apply large normal forces to the wearer (in order to impart pressure). Therefore, to mitigate high friction and, therefore, increase pressure uniformity while still maintaining large normal forces, the coefficient of friction must be reduced. This can be accomplished by changing the surface finish of the passive fabric by introducing a slip layer garment to facilitate donning (as previously recommended by Anis and Webb[4] and Waldie et al.[31]), or by introducing a lubricating agent (such as petroleum jelly) to facilitate nonstick behavior.

For ease of testing (and for repeatability purposes), the tests conducted in this study used a simple PVC pipe, which differs significantly from an actual human limb (which is neither regularly shaped nor made from a homogeneous, rigid material). Consequently, it is necessary to assess the effect that these differences will have on system performance when donned on an actual human (or other soft/irregular object):

1. If the friction coefficient of human skin differs significantly from the friction coefficient of the PVC pipe or the Novel pressure sensor, this difference will affect the spatial variability of the passive and active pressure profiles. The friction coefficient of human skin varies, ranging from $0.12 < \mu < 0.34$, depending on anatomical region (averaging approximately $\mu = 0.21$).[9] The coefficient of friction for PVC is reported to be $\mu = 0.2–0.3$.[12] These values are comparable to one another (so the effect is likely minimal), but without a detailed experiment, we cannot explicitly quantify this uncertainty.
2. The thin-walled hoop stress equation relates tension, pressure, and local radius.[3] If the local radius of curvature varies along the circumference of a given limb, the local garment tension will also likely vary due to friction between the garment and the wearer (preventing the local fabric tension from equilibrating through the full garment). The net effect on counterpressure will depend on both the changes in radius and tension at a given location. In a hypothetical scenario where friction is negligible, tension will not vary spatially despite local changes in radius, creating a spatially dependent pressure profile that varies proportionally to the local radius.
3. The difference in rigidity and local curvature between PVC and human tissue will affect both the total pressure and the spatial pressure distribution. Depending on the body location of the active garment, the nature of the underlying tissue may vary wildly; for example, if placed on the front of the shin, where the tibia sits just beneath the surface, the system dynamics will differ from a similar test conducted on the upper thigh, where thick muscle tissue exists around the full circumference in roughly cylindrical form. Young's modulus values for human tissue vary: muscle tissue modulus averages between 1-3 kPa,[8] which differs greatly from dry collagen (6 GPa) and bone (5-21 GPa).[30] The Young's modulus of PVC, on the other hand, varies between 2-4 GPa,[13] which is similar to bone. We therefore expect a significant change in system dynamics if the system is tested over irregular, soft tissue regions (with applied pressure causing a decrease in radius, in turn causing a decrease in transient tension and pressure and a greater-than-predicted SMA contraction stroke). This quasi-static process will likely continue until equilibrium is reached between the applied pressure and the tissue elastic response.

Quantifying these effects was beyond the scope of this study; however, if an effective modulus value can be determined for each body location (perhaps representing a weighted average of moduli values reflecting the relative proportion of soft and hard tissue at that location), then we can calculate the relationships between applied pressure, effective tissue modulus, and effective limb radius. These relationships for effective radius could be incorporated into the predictive model—treating limb radius as a variable quantity based on pressure and effective limb modulus, rather than as a static quantity—to predict passive and active pressures for soft surfaces. However, this will be further complicated by the fact that human limbs are not perfect cylinders and the radius of curvature varies both circumferentially and longitudinally.

Finally, we recognize that this study has limitations that warrant discussion.

1. SMA actuators themselves have limitations that will affect the systems in which they are used. The SMA frequency response is low, relative to other active materials, which limits their performance in highly dynamic systems.[5] The systems proposed and studied in this effort are effectively two-state, static systems, and the actuators are used to transition from one static state (the passive pressure condition) to another static state (the active pressure condition). Should it be desired for the compression garment to dynamically function, either as a powered support device or to morph or otherwise augment the wearer during motion, then the choice of SMA coil actuators as presented may be suboptimal.
2. SMA actuators are notoriously power hungry and hysteresis prone: the system tested in this study required 27 W of power for 9 s to achieve MCP pressure targets over a 3.81-cm width. Designs that can capture the tension created during SMA activation (through a locking, lacing, or similar architecture), enabling the actuators to be deactivated once a target counterpressure has been reached, should be prioritized and investigated.
3. The performance tests conducted in this study used a rigid cylindrical object (PVC pipe) as the base structure against which pressure was produced. Humans are not rigid cylindrical objects and soft tissue will not necessarily respond in the same fashion when exposed to an applied pressure. Subsequent system testing on nonrigid objects (ideally on human subjects) is a critical next step in system validation.
4. The sleeve prototypes developed for this study were not full garments. Each prototype was only 1.5" wide (resembling a cuff rather than a full sized sleeve). However, the technology and predictive model are both modular, enabling similar full-sized garments to be modeled and constructed by simply adding more actuator modules in parallel along the limb axis. We did not construct or test a full-sized garment, but we expect the performance of such a garment to mimic the performance of the prototypes developed in this study.
5. Finally, we observed limitations in system performance that can be attributed simply to limitations in design, manufacturing, or material selection. The passive fabrics were chosen based on commercial availability and not on optimized performance, and breakdowns in their characteristics (i.e., irrecoverable strain, loss of modulus, nonlinear behavior, and high friction) affected the test results. Similarly, the 3D printed actuator cartridges, as designed, contributed to the "near-field" pressure distortion and experienced structural failure at high tensions that limited the system durability and the maximum pressures observed. More detailed consideration of these system aspects is warranted.

The active sleeve tests conducted in this study provide significant insight into future active compression garment design. The hybrid systems developed for these tests exhibited considerable counterpressure increases as a result of the novel SMA coil actuator cartridge system, and it was demonstrated that this increase in performance can achieve MCP target pressures and can be triggered quickly. To the best of our knowledge, these tests represent the first widespread testing of a controllable, active compression garment that uses integrated SMA coil actuators, and their successful performance provides credibility to the claim that SMA-based active garments are well suited for compression garment applications, including space medicine (e.g., preventing orthostatic intolerance) and extravehicular activity (e.g., enabling easy-to-don MCP space suits).

ACKNOWLEDGMENTS

The authors would like to thank our colleagues at NASA Johnson Space Center, NASA Langley Research Center, NASA Jet Propulsion Laboratory, U.S. Army Natick Soldier Systems Center, and MIT for their support and collaboration. This work was supported by a NASA OCT Space Technology Research Fellowship (NASA Grant NNX11AM62H) as well as the MIT Portugal Program.

Authors and affiliations: Bradley T. Holschuh, Ph.D., and Dava J. Newman, Ph.D., Department of Aeronautics and Astronautics, Massachusetts Institute of Technology, Cambridge, MA.

REFERENCES

1. Abel J, Luntz J, Brei D. Hierarchical architecture of active knits. Smart Mater Struct. 2013; 22(12):125001.
2. An SM, Ryu J, Cho M, Cho KJ. Engineering design framework for a shape memory alloy coil spring actuator using a static two-state model. Smart Mater Struct. 2012; 21(5):055009.
3. Anderson A. Addressing design challenges in mechanical counterpressure spacesuit design and space-inspired informal education policy. Masters Dissertation. Cambridge (MA): Department of Aeronautics and Astronautics, Massachusetts Institute of Technology; 2011.
4. Annis JF, Webb P. Development of a space activity suit. Washington (DC): NASA; 1971. Report No.: NASA-CR-1892.
5. Bell D, Lu T, Fleck N, Spearing S. Mems actuators and sensors: observations on their performance and selection for purpose. J Micromech Microeng. 2005; 15(7):S153.
6. Berzowska J, Coelho M. Kukkia and vilkas: kinetic electronic garments. 9th IEEE International Symposium on Wearable Computers. Piscataway (NJ): IEEE; 2005:82-85.

7. Brennan MJ, Miller LT. Overview of treatment options and review of the current role and use of compression garments, intermittent pumps, and exercise in the management of lymphedema. Cancer. 1998; 83(Suppl. 12B):2821–2827.
8. Chen EJ, Novakofski J, Jenkins WK, O'Brien WD, Jr. Young's modulus measurements of soft tissues with application to elasticity imaging. IEEE Transactions on Ultrasonics, Ferroelectrics and Frequency Control. 1996; 43(1):191–194.
9. Cua AB, Wilhelm K, Maibach H. Frictional properties of human skin: relation to age, sex and anatomical region, stratum corneum hydration and transepidermal water loss. Br J Dermatol. 1990; 123(4):473–479.
10. Diehm C, Trampisch H, Lange S, Schmidt C. Comparison of leg compression stocking and oral horse-chestnut seed extract therapy in patients with chronic venous insufficiency. Lancet. 1996; 347(8997): 292–294.
11. Doan BK, Kwon YH, Newton RU, Shim J, Popper EM, et al. Evaluation of a lower-body compression garment. J Sports Sci. 2003; 21(8):601–610.
12. Engineering Plastic Products DOTMAR. 2014. Coefficient of friction of plastics [Accessed 20 April 2014]. Available from http://www.dotmar.com.au/co-efficient-of-friction.html.
13. Engineering ToolBox. 2014. Tensile modulus for common materials [Accessed 14 April 2014]. Available from http://www.engineeringtoolbox.com/young-modulus-d_417.htm.
14. Holschuh B, Newman D. Low spring index, large displacement shape memory alloy (SMA) coil actuators for use in macro-and micro-systems. In: SPIE MOEMS-MEMS. Bellingham (WA): International Society for Optics and Photonics; 2014:897505.
15. Holschuh B, Newman D. Two-spring model for active compression textiles with integrated ni-ti coil actuators. Smart Mater Struct. 2015; 24(3):035011.
16. Holschuh B, Obropta E, Buechley L, Newman D. Materials and textile architecture analyses for mechanical counter-pressure space suits using active materials. In: AIAA Space 2012 Conference Expo. Pasadena (CA): AIAA; 2012.
17. Holschuh B, Obropta E, Newman D. Low spring index niti coil actuators for use in active compression garments. IEEE Transactions on Mechatronics. 2014; 20(3):1264-1277.
18. Holschuh BT. Mechanical counter-pressure space suit design using active materials. [Ph.D. Dissertation.] Cambridge (MA): Department of Aeronautics and Astronautics, Massachusetts Institute of Technology. 2014.
19. Judnick D, Newman D, Hoffman J. Modeling and testing of a mechanical counterpressure bio-suit system. Warrendale (PA): SAE International; 2007. SAE Technical Paper, pages 2007–01–3172.
20. Kim S, Hawkes E, Cho K, Jolda M, Foley J, Wood R. Micro artificial muscle fiber using niti spring for soft robotics. In: 2009 IEEE/RSJ International Conference on Intelligent Robots and Systems. Piscataway (NJ): IEEE; 2009:2228–2234.
21. Kragh JF Jr, Littrel ML, Jones JA, Walters TJ, Baer DG, et al. Battle casualty survival with emergency tourniquet use to stop limb bleeding. J Emerg Med. 2011; 41(6):590–597.
22. Lagoudas DC. Shape memory alloys: modeling and engineering applications. Berlin: Springer; 2008.
23. Madden J, Vandesteeg N, Anquetil P, Madden P, Takshi A, et al. Artificial muscle technology: physical principles and naval prospects. IEEE Journal of Oceanic Engineering. 2004; 29(3):706–728.
24. Newman D, Hoffman J, Bethke K, Carr C, Jordan N, et al. Astronaut bio-suit system for exploration class missions. Atlanta (GA): NIAC; 2005. NIAC Phase II Final Rep. Available at http://www.niac.usra.edu/files/studies/final_report/833Newman.pdf.
25. Platts SH, Tuxhorn JA, Ribeiro LC, Stenger MB, Lee S, Meck JV. Compression garments as countermeasures to orthostatic intolerance. Aviat Space Environ Med. 2009; 80(5):437–442.
26. Seok S, Onal CD, Cho K-J, Wood R, Rus D, Kim S. Meshworm: a peristaltic soft robot with antagonistic nickel titanium coil actuators. IEEE/ASME Trans Mechatron. 2012; 18(5):1485–1497.
27. Stenger MB, Brown AK, Lee S, Locke JP, Platts SH. Gradient compression garments as a countermeasure to post-spaceflight orthostatic intolerance. Aviat Space Environ Med. 2010; 81(9):883–887.
28. Stenger MB, Lee S, Westby CM, Ribeiro LC, Phillips TR, et al. Abdomen-high elastic gradient compression garments during post-spaceflight stand tests. Aviat Space Environ Med. 2013; 84(5):459–466.
29. Teng T-L, Chou K-T. The measurement and analysis of the pressure generated by burn garments. J Med Biol Eng. 2006; 26(4):155–159.
30. University of Cambridge. 2004. Mechanical properties of bone [Accessed 14 April 2014]. Available from http://www.doitpoms.ac.uk/tlplib/bones/bone_mechanical.php.
31. Waldie JM, Tanaka K, Tourbier D, Webb P, Jarvis CW, Hargens AR. Compression under a mechanical counter pressure space suit glove. J Gravit Physiol. 2002; 9(2):93–97.
32. Webb P, Annis J. The principle of the space activity suit. Washington (DC): NASA; 1967. NASA CR-973.
33. Yuen M, Cherian A, Case JC, Seipel J, Kramer RK. Conformable actuation and sensing with robotic fabric. In: 2014 IEEE/RSJ International Conference on Intelligent Robots and Systems (IROS 2014). Piscataway (NJ): IEEE; 2014:580–586.